LETTER

Rethinking Oxygen Redox: Does Oxygen Dimerization Occur without Oxidation in Li₂NiO₃?

Matthew J. W. Ogley, Ashok S. Menon,* Beth J. Johnston, Gaurav Pandey, Innes McClelland, Xiaoqun Shi, Stefano Agrestini, Veronica Celorrio, Gabriel E. Pérez, Samuel G. Booth, Jordi Cabana, Serena A. Cussen, and Louis F. J. Piper*

Read Online

ACCESS | 📊 Metrics & More | 📖 Article Recommendations | 🆘 Supporting Information

ABSTRACT: In layered lithium transition metal oxide cathodes, high-voltage operation is accompanied by the formation of oxygen dimers, which are widely used as an indicator of oxygen-redox activity. However, understanding the role that oxygen dimerization plays in facilitating charge compensation is still needed. Li_2NiO_3 (a $3d^8\underline{L}^2$-containing compound, where $\underline{L}$ is a ligand hole) is studied as a model system, where oxygen dimerization is shown to occur without cathode oxidation. Electrochemical cycling results in a net reduction of the cathode, accompanied by structural transformations, despite spectroscopic features of oxygen dimers arising at the top-of-charge. Here, oxygen dimerization is shown to coexist alongside a structurally transformed and electronically reduced cathode structure, thus highlighting that O dimerization is independent of bulk redox processes. This makes it clear that a thermodynamically derived transformation toward a reduced phase remains the only variable capable of generating O−O dimers in Li_2NiO_3.
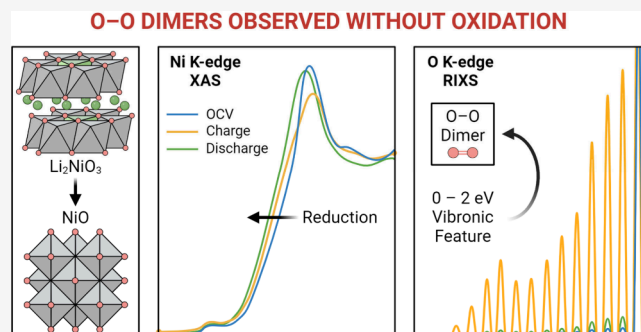
Considering the role Ni plays in promoting O loss and subsequent degradation in transition metal (TM) oxide Li-ion battery cathodes (LiTMO₂),[1−3] studying their charge compensation mechanism has become ever-more important.[4−6] Progress on the topic has contested the applicability of conventional oxidation state nomenclature to Ni-containing TM oxide cathodes.[7−11] Here, O has been shown to dominate the redox process during (de)lithiation, resulting in the formation of $3d^8\underline{L}$ and $3d^8\underline{L}^2$ electronic states, where $\underline{L}$ is a ligand hole.[12,13] In such cathodes, bulk sensitive TM K-edge X-ray absorption spectroscopy (XAS) data stops linearly evolving at high voltages,[13] marking a regime where delithiation no longer results in a net change to the TM−O bond length.[14−17] Interestingly, beyond this regime, O K-edge resonant inelastic X-ray scattering (RIXS) data has revealed the growth of neutral 1.2-Å O−O dimers, which has been hitherto ascribed to O oxidation.[14,18−21] Therefore, it becomes necessary to identify the role that the O−O dimer species play, if any, in the underlying capacity contributions of such cathodes.

Understanding the origin of O dimerization requires consideration of the routes through which O−O dimer species may be formed during delithiation. Layered LiTMO₂ systems

are thermodynamically unstable.[22,24,25] During delithiation, they have an intrinsic thermodynamic propensity to undergo a layered to rock salt structural transformation that results in the formation of O₂.[25,26] As shown in Figure 1a, the delithiation of LiNiO₂ toward NiO₂ encompasses no thermodynamically stable states and all partially delithiated phases will tend to reconstruct to form LiNiO₂, NiO and O₂ in a given ratio (Figure 1b).[22,26−28] While this process is kinetically slow, the structural transformations can be accelerated by the presence of crystallographic defects,[25,29−32] and recent computational works have predicted that these defects also provide domains where O−O dimers may be generated locally.[19,33] Li₂NiO₃ shares the thermodynamic characteristics of LiNiO₂; all partially delithiated phases will thermally reconstruct and form O₂ (Figure 1c).[23] However, unlike stoichiometric
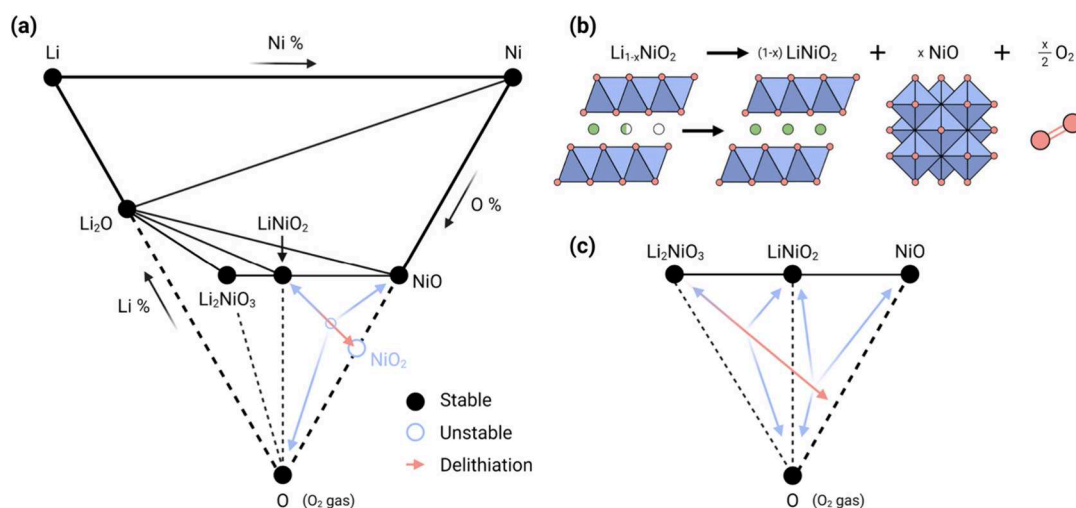
Figure 1. (a) Ternary Li−Ni−O phase diagram outlining the delithiation pathway (red arrow) of $LiNiO_2$ toward NiO_2. Filled black and unfilled blue circles represent stable and unstable compounds, respectively. The thermodynamic propensity for partially delithiated phases to undergo reconstruction is illustrated with blue arrows. Dashed black lines indicate a dependence on O_2 partial pressure. Reproduced from ref 22. Copyright 2007 American Chemical Society. Adapted from ref 23. Available under a CC-BY 4.0. Copyright 2023 IOP Publishing. (b) Balanced chemical equation describing the thermal decomposition of layered $Li_{1−x}NiO_2$ (where $0 < x \leq 1$) to form $(1−x)$ $LiNiO_2$, x NiO and $\frac{x}{2}$ O_2. (c) Li_2NiO_3−NiO−O_2 subtriangle from (a) illustrating the predicted delithiation pathway of Li_2NiO_3 and the instability of all partially delithiated phases.
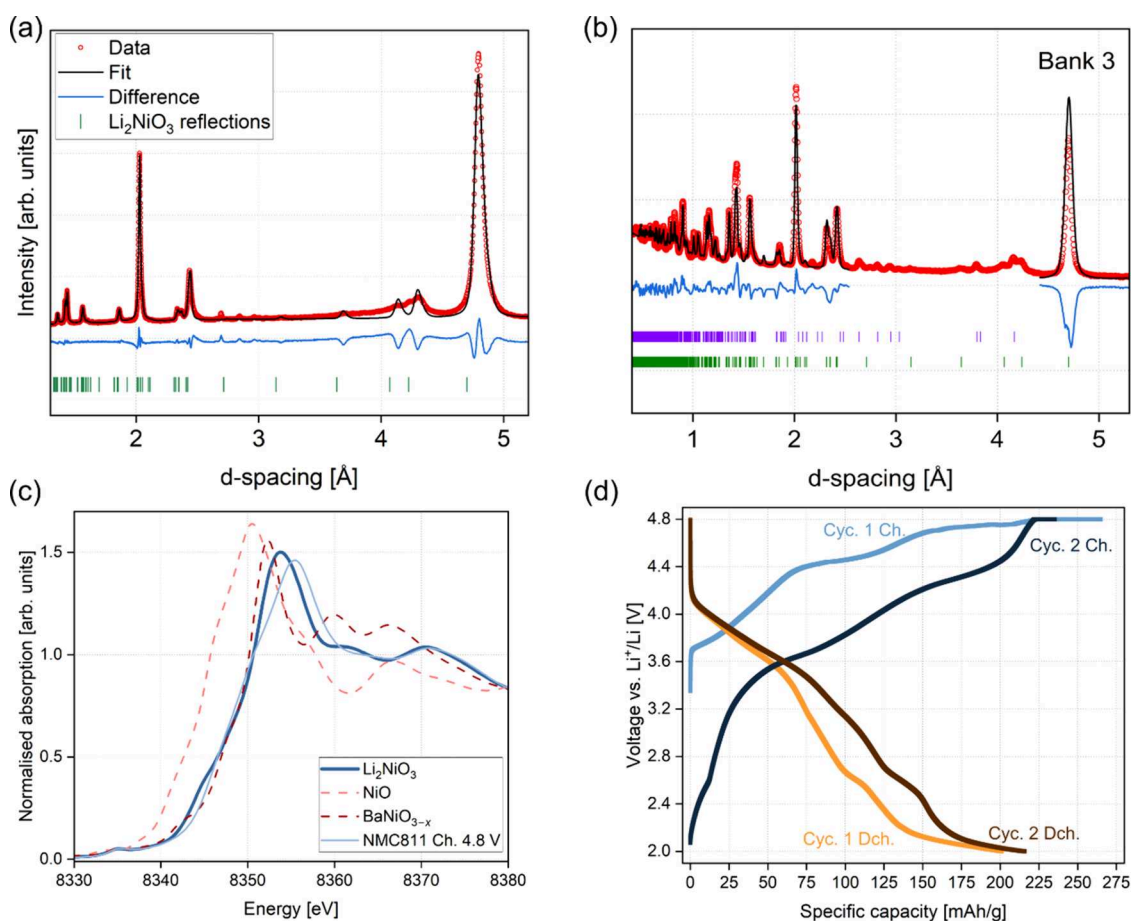
Figure 2. X-ray (a) and neutron (b) diffraction data fits of the pristine Li_2NiO_3 sample. The neutron diffraction data were collected from bank 3 of the Polaris diffractometer. The purple markers in (b) are solely used to illustrate the positions of Li_2CO_3 ($C2/m$) reflections; they were not included in the refinements, as the 2.45−4.44 Å 'superstructure' region was not included in the refinements. (c) Ni K-edge XANES data of NiO, Li_2NiO_3, $BaNiO_{3−x}$, and charged (4.8 V) NMC811. (d) Voltage vs specific capacity profiles of the first two cycles of Li_2NiO_3 cycled against Li between 2 and 4.8 V at a C/20 rate.

$LiTMO_2$ cathodes where delithiation-induced transformations occur alongside electronic charge compensation processes, further oxidation of the NiO_2-like $3d^8\underline{L}^2$ ground state is not expected. This makes Li_2NiO_3 an excellent model system to investigate the link between delithiation, oxidation, and O−O dimer formation. Furthermore, it also helps to contextualize the behavior of highly delithiated Ni-rich $LiTMO_2$ cathodes at high voltages.

Herein, the changes in the electronic structure of Li_2NiO_3, together with its delithiated (charged) and relithiated (discharged) states were investigated using multiscalar X-ray spectroscopic methods. Bulk and surface trends were identified, and in both cases only a net irreversible reduction of the cathode was observed. Nevertheless, O−O dimers were observed at the top-of-charge before disappearing upon discharge. The same reductive trends and reversible O dimerization were also observed to persist upon prolonged cycling. These observations raise questions about its mechanistic origin with respect to delithiation.

Li_2NiO_3 was synthesized through the high temperature annealing of a $LiOH.H_2O$ and $Ni(OH)_2$ mixture in an O_2 atmosphere. Inductively coupled plasma - optical emission spectrometry (ICP-OES) analysis determined the Li:Ni ratio to be 1.97:1.03, and hence, is comparable to the intended value. As observed through scanning electron microscopy, the particles were of a polycrystalline morphology (Figure S1). Figure 2a and Figure 2b show the X-ray and neutron diffraction data fits of the as-synthesized sample, respectively. Li_2NiO_3 is isostructural to Li_2MnO_3 and crystallizes in a monoclinic ($C2/m$) structure with alternating Li and Li−Ni layers within a ccp O framework. This is evidenced by the presence of superstructure reflections in the diffraction data, formed by the hexagonal ordering of the Li and Ni cations in the Li−Ni layer. Fitting a $C2/m$ unit cell to the XRD data (Figure 2a) yielded lattice parameter values comparable to previous reports (refined unit cell parameters in Table S1).[34,35] Similar to these works, the Li_2NiO_3 sample also contained additional phases such as Li_2O, Li_2CO_3 and LiOH. Nevertheless, Rietveld refinement of a $C2/m$ Li_2NiO_3 structure model (Figure 2b) against time-of-flight neutron diffraction data indicates that the desired phase has been obtained. Additional neutron diffraction data fitting, which supports this conclusion is shown in Figure S2, with the refined parameters in Table S2. Note that the additional phases and the anisotropic broadening of the superstructure reflections (due to stacking faults) preclude a reliable quantitative structural analysis. Perhaps more pertinent to this work is that the formal oxidation state of Li_2NiO_3, based on the Ni K-edge spectra, is very close to that of a highly delithiated $LiNi_{0.8}Mn_{0.1}Co_{0.1}O_2$ (NMC811) cathode charged to 4.8 V (vs Li^+/Li).[13] This is evident from Figure 2c, where the Ni K-edge X-ray absorption near edge spectroscopy (XANES) data of these two compounds are compared with NiO ($3d^8$) and $BaNiO_{3-x}$ ($3d^8\underline{L}^2$). Note that $BaNiO_{3-x}$, like 4.8-V NMC811 and Li_2NiO_3 is highly oxidized and likely to be O deficient.[13,36] Furthermore, the Ni−O bond length calculated from the corresponding Fourier-transformed extended X-ray absorption fine structure (EXAFS) data (1.873(8) Å, Figure S3 and Table S3) is the same as 4.8-V NMC811 (1.873(5) Å),[13] confirming that the overall electronic structure is close to $3d^8\underline{L}^2$ and that it is ideal for the objective of this work.

The first and second cycle galvanostatic charge−discharge profiles of Li_2NiO_3 cycled against metallic Li at C/20 rate is shown in Figure 2d. Unlike Li_2MnO_3, Li_2NiO_3 demonstrates a sloping profile, providing a capacity of approximately 220 mAh/g before reaching 4.8 V. Significant capacity continues to be extracted during the current-limited 4.8-V constant voltage step, yielding a total capacity of approximately 250 mAh/g. Previous work has shown that the delithiation/charging is accompanied by significant O_2 and CO_2 evolution beyond 4.4 V and interestingly, Li_2NiO_3 releases twice as much O_2 when compared to Li_2MnO_3.[34,37] Upon discharge, it demonstrates a sizable capacity loss of approximately 50 mAh/g and a large voltage hysteresis during the subsequent discharge. In Li_2MnO_3 and its doped variants, first cycle electrochemical degradation is attributed to O loss and the associated irreversible structural transformations that occur during charge.[37,38] The former is stated to occur due to the oxidation of nonbonding O 2p orbitals located along the Li−O−Li configurations present within layered Li-excess structures.[39] This oxidation is then thought to promote bulk TM migration, both within and between the TM layers, thus forming vacancy clusters.[21,40] In Li-rich Ni−Mn−Co oxide cathodes, these clusters have been shown to contain 1.2-Å long O−O dimers, as evidenced through O K-edge RIXS experiments.[21,41] In our recent works, we have shown that the same RIXS features, and by extension the same oxidized O species, form in W-doped $LiNiO_2$, NMC811, and $LiCoO_2$, none of which possess long-range Li−O−Li bonding configurations, or undergo the same delithiation-induced structural transformations that have been reported for Li-rich systems.[13,14,21] This implies that O dimerization does not depend on the Li−O−Li environments as previously proposed.

Upon cycling, there is a significant transformation of the discharge profiles in the first, second and 25th cycles (Figure S4), suggesting the gradual structural transformation of the Li_2NiO_3 cathode. Nevertheless, the capacity values obtained during the initial and 25th C/20 cycles are similar. Figure S5 demonstrates that the capacity is strongly rate dependent; increasing the cycling rate to C/2 in the third cycle halves the practical capacity. A monotonic capacity fade of 50% is observed in the next 20 C/2 cycles, after which the capacity climbs back in the 25th (C/20) cycle. Taken together, it is clear that the cycling leads to significant changes in the crystallographic (and by extension, electronic) structure of Li_2NiO_3. Furthermore, the reactivity of the highly oxidized Ni−O environments is likely to promote a surface-to-bulk gradient in the cathode structure. Due to the interplay between electronic structure and charge compensation, these differences are worth investigating.

Bulk-to-surface differences are evident in the fluorescent yield (FY, Figure 3a) and electron yield (EY, Figure 3b) Ni L-edge XAS data. This shows the Ni−O hybridized states of the open circuit voltage (OCV) sample getting progressively reduced toward the surface, reminiscent of $LiNiO_2$ and NMC811.[13,15,19] Based on our previous study, the valence states of pristine NMC811 are closer to $3d^8\underline{L}^2$ in the bulk but closer to $3d^8$ at the surface.[13] Intriguingly, at the end of charge where oxidation is expected, counterintuitively, a net reduction has occurred. This is evidenced by the decreasing intensity of peak B (w.r.t. peak A) and reduction of the ≈866-eV $3d^8\underline{L}^2$ charge-transfer feature (Peak C). This trend is not reversible and further reduction has occurred during discharge, as reported previously.[34] Furthermore, the same reductive behavior is also observed to continue in the 25th cycle (Figures S6 and S7). Regarding the first-cycle data, to abate
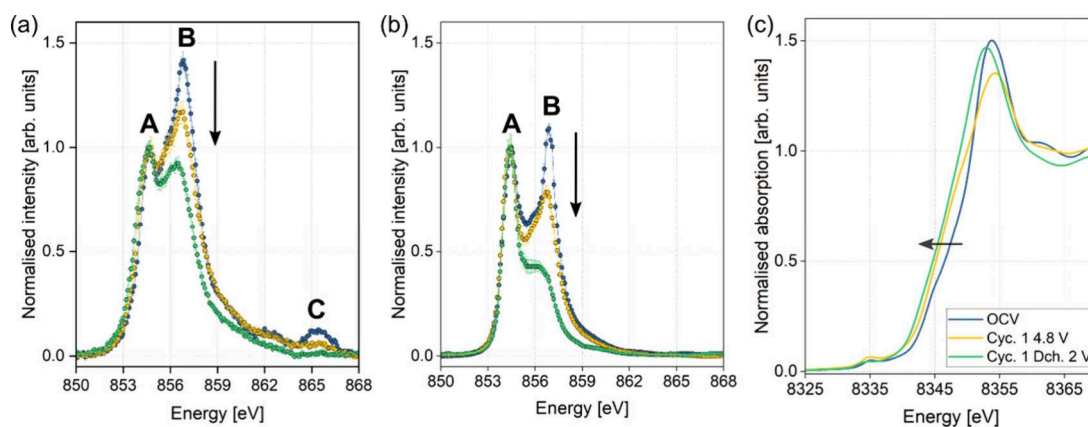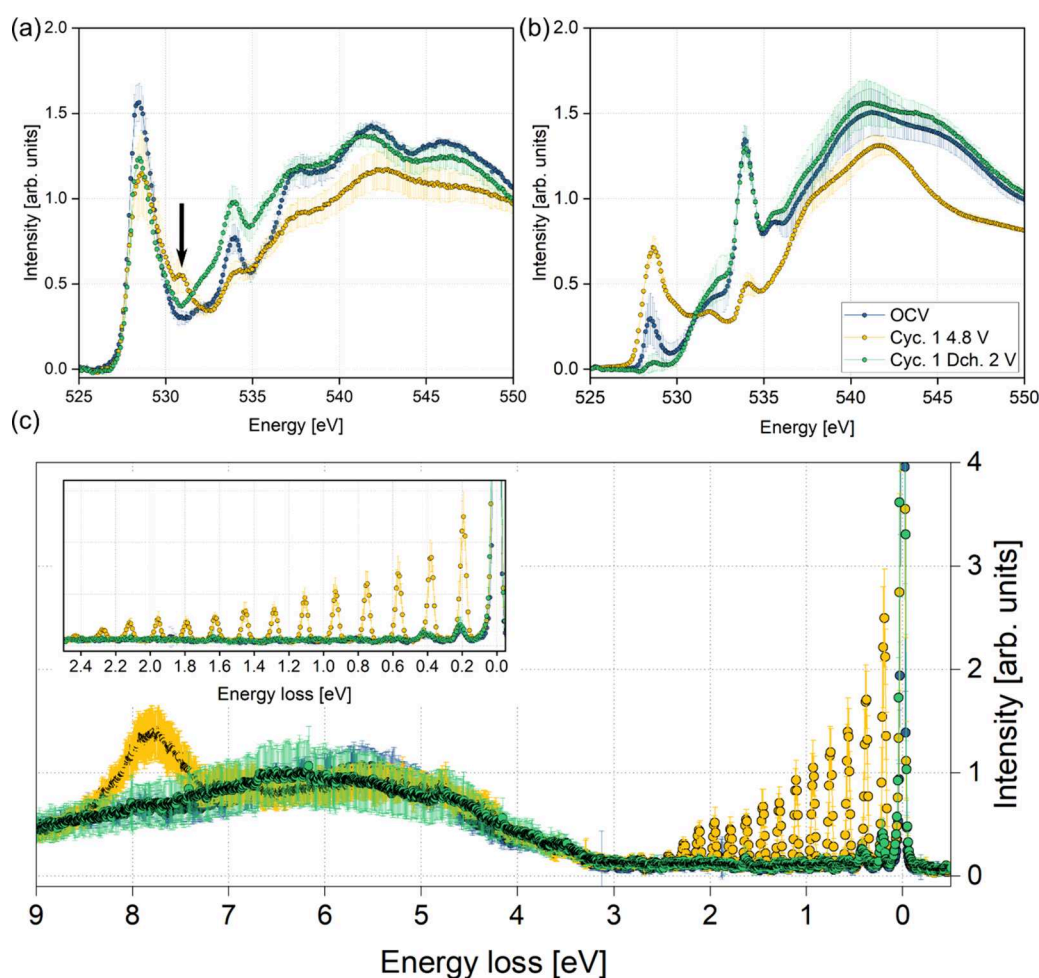
Figure 3. Background-subtracted, normalized Ni L_3-edge spectra of Li_2NiO_3 collected in (a) fluorescence (FY) and (b) electron (EY) yield modes. The three important spectral features are labeled A, B, and C. (c) Ex-situ Ni K-edge XANES spectra of Li_2NiO_3. The legend in plot (c) applies to all plots.

any ambiguity about the degree of bulk sensitivity of the FY data, bulk-sensitive transmission Ni K-edge XANES measurements are shown in Figure 3c and display the same reductive trend. Ni K-edge XANES data for all samples and standards are shown in Figure S8. A shift toward lower energies is clearly observed for the charged and discharged samples. The same trends are observed in the Ni K-edge EXAFS data (Figures S9, S10, and S11) where the decreasing intensity of the Ni−O coordination shell represents reduction.[42] Note that the OCV data presented here is the same as the one in Figure 2c. This reductive behavior is also supported by diffraction data in ref 34 where it was demonstrated that the parent layered structure gradually transforms into a cubic rock salt structure over the course of cycling. Considering that ligand holes, present on O, are responsible for driving charge compensation and reactivity in this material, further scrutiny of the electronic structure of O is necessary.

In the O K-edge XAS (Figures 4a and 4b), dipole selection rules afford sensitivity to the hybridized TM−O valence band, as well as any unfilled unhybridized O orbitals that may be present due to Li−O−Li configurations (previously believed to promote O-redox activity) in the Li_2NiO_3 structure. Here, the intensity of the pre-edge peak ($\approx$529 eV) evolves differently depending on the probe depth. In the bulk-sensitive FY data, the intensity has decreased at the top-of-charge, thus signifying the reduction of TM−O hybridized states. This is barely reversible during discharge, with the pre-edge peak intensity remaining invariant. The same trends are not observed in the EY data and misleadingly appear to evolve conventionally, whereby the pre-edge peak intensity should increase during charge (creation of ligand holes) before decreasing upon discharge (filling of ligand holes). However, the observed trend is unlikely to be due to changes in TM−O hybridization alone. In the pristine sample, the presence of a thick Li_2CO_3 surface layer, verified through observation of the 534-eV peak,[43] is likely to artificially suppress the pre-edge peak intensity. When in the charged state, the intensity of the Li_2CO_3 peak is substantially weaker, representing its decomposition at high voltages. Consequently, a newly "clean" surface reveals a Ni−O-containing environment that exhibits the expected ligand hole-containing, pre-edge peak-promoting electronic environment. During discharge, a drastic reduction of that pre-edge peak occurs. Now, two factors likely contribute to this diminished intensity: the formation of rock salt NiO, which

does not exhibit a peak at 529 eV,[44] and the reformation of Li_2CO_3, observed through the reversible formation of the peak at 534 eV. Support for both variables affecting the O K-edge is found through inspection of the data from the 25th cycle (Figure S12 and S13). Here, between charge and discharge, changes in the pre-edge peak intensity have occurred. If solely NiO were present, no changes would be expected during electrochemical (de)lithiation.

In the context of "O-redox", perhaps the most interesting feature of the FY O K-edge is, as before, the decreasing pre-edge peak intensity (signifying the reduction of hybridized states), but also the accompanying increase in spectral intensity at $\approx$531.3 eV, highlighted in Figure 3a using an arrow. This peak corresponds to the 1s → π^* absorption of a neutral O−O dimer,[5,20,45] a species shown to exist in a wide range of highly oxidized TM oxide cathodes.[13,14,18,19] Figure 4c shows 531.3-eV O K-edge RIXS spectra collected on Li_2NiO_3 cathodes at OCV, charged (4.8 V) and discharged (2 V) states. Unlike the previous XAS data, the RIXS data shows reversible trends. In the charged state, a strong growth of vibronic 0−2 eV features, with the first two peaks separated by $\approx$0.192 eV ($\approx$1550 cm^{-1}), are attributed to neutral O−O dimers that disappear on discharge.[21] The same behavior is also observed in the 25th cycle RIXS data (Figures S14 and S15). While it is difficult to draw quantitative conclusions on O−O dimer concentration using RIXS data alone, evidently their formation is neither proportional nor concomitant to, ligand hole formation. This is illustrated by the high intensity of the 8-eV and 0−2-eV RIXS features in the charged Li_2NiO_3 sample, while the number of holes in the hybridized O 2p−TM 3d states is clearly decreasing as shown in the O K-edge and Ni L-edge XAS data. In contrast to the RIXS spectra of $LiNiO_2$ and $LiNi_{0.8}Mn_{0.1}Co_{0.1}O_2$,[14,19] there is a notable absence of a 5 eV energy loss feature.[13,14,19] This feature is absent in the RIXS spectra of O_2 gas,[20] and must therefore be attributed to changes in the Ni−O hybridization. Its absence at any state-of-charge in Li_2NiO_3 further emphasizes the absent oxidation of hybridized valence states. It is worth highlighting that very weak vibronic features are also observed in the OCV and discharged samples, with initial peak spacings of $\approx$0.21 eV (Figure S16). These features may represent a C=O bond ($\approx$1700 cm^{-1}) from within Li_2CO_3, a species known to be present from the O K-edge XAS data. However, given that there are an insufficient number of clearly resolved vibronic

Figure 4. Background-subtracted, normalized O K-edge data obtained from the Li_2NiO_3 electrodes collected in (a) FY and (b) EY modes. (c) RIXS spectra of the Li_2NiO_3 electrodes collected at $\approx$531.3 eV. The vibronic features (0–2 eV) are magnified in the top left inset. The legend in plot (b) applies to all plots.

peaks, an accurate characterization is prevented. Returning to the O−O dimer feature, in comparison to delithiated $LiNiO_2$ and $LiNi_{0.8}Mn_{0.1}Co_{0.1}O_2$ (where $3d^8\underline{L}^2$ dominates),[13,19] its absence in the OCV Li_2NiO_3 sample, supposedly with the same electronic configuration, is intriguing. This suggests that Li content is a key determinant in driving the intensity of the RIXS feature. This can be best highlighted using Li_2NiO_3 alone, where the intensity of the 8-eV and 0–2-eV features is increased with delithiation (charge) and decreased with relithiation (discharge) despite a net reduction of the cathode occurring in both cases. Upon discharge, no gas evolution occurs in Li_2NiO_3.[34] This would suggest that incoming Li^+ reacts with bulk O−O dimers when reintegrating into the cathode structure. To summarize for Li_2NiO_3, O−O dimers are observed in the presence of reduced Ni−O environments, do not necessarily accompany $3d^8\underline{L}^2$ states, and arise only upon delithiation. This implies that O−O dimers are a byproduct of the structural change that arises due to the thermal instability of the partially delithiated structure, a factor which encourages O dimerization and the formation of reduced phases. Through observations of the 531-eV RIXS features in other stoichiometric and Li-rich layered oxide cathodes,[13,14,21,46] this process seemingly occurs independently of the electronic environment.

Further support for this comes from revisiting the delithiation mechanism of spinel $Li_{1-x}Ni_{0.5}Mn_{1.5}O_4$. Similar

to layered Ni-containing $LiTMO_2$ and Li-rich Ni-containing NMC cathodes, delithiation is charge compensated through the formation of $3d^8\underline{L}^2$ states,[47] with the Ni−O bond length plateauing toward the top-of-charge.[48] While this may lead one to expect behavior similar to stoichiometric $LiTMO_2$ cathodes, $Li_{1-x}Ni_{0.5}Mn_{1.5}O_4$ does not undergo any structural transformations that result in the formation of a reduced phase.[49] Consequently, neither gas evolution[50] nor 531-eV O K-edge vibronic RIXS features are observed.[51]

Using Li_2NiO_3, we investigated a model layered oxide system that undergoes reduction during (de)lithiation, and still exhibits the 531-eV RIXS features at the top-of-charge (4.8 V vs Li^+). This study reveals that redox processes are independent of bulk O−O dimerization. It confirms that the thermodynamically derived transformation toward a reduced rock salt phase is the cause of O−O dimer formation.

■ ASSOCIATED CONTENT

ⓢ Supporting Information

The Supporting Information is available free of charge at https://pubs.acs.org/doi/10.1021/acsenergylett.4c02031.

> Experimental details, microscopy, ex-situ diffraction and spectroscopy fittings, electrochemistry, Ni L-edge XAS, Ni K-edge XAS, O K-edge XAS, O K-edge RIXS, Birge−

Sponer plot, and diffraction refinement parameters (PDF)

■ AUTHOR INFORMATION

Corresponding Authors

Louis F. J. Piper − *Warwick Manufacturing Group, University of Warwick, Coventry CV4 7AL, U.K.; The Faraday Institution, Didcot OX11 0RA, U.K.;* ● orcid.org/0000-0002-3421-3210; Email: Louis.Piper@warwick.ac.uk

Ashok S. Menon − *Warwick Manufacturing Group, University of Warwick, Coventry CV4 7AL, U.K.; The Faraday Institution, Didcot OX11 0RA, U.K.;* Email: Ashok.Menon@warwick.ac.uk

Authors

Matthew J. W. Ogley − *Warwick Manufacturing Group, University of Warwick, Coventry CV4 7AL, U.K.; The Faraday Institution, Didcot OX11 0RA, U.K.*

Beth J. Johnston − *Warwick Manufacturing Group, University of Warwick, Coventry CV4 7AL, U.K.; The Faraday Institution, Didcot OX11 0RA, U.K.*

Gaurav Pandey − *Warwick Manufacturing Group, University of Warwick, Coventry CV4 7AL, U.K.*

Innes McClelland − *The Faraday Institution, Didcot OX11 0RA, U.K.; Department of Materials Science and Engineering, The University of Sheffield, Sheffield S1 3JD, U.K.;* ● orcid.org/0000-0001-9821-715X

Xiaoqun Shi − *The Faraday Institution, Didcot OX11 0RA, U.K.; Department of Materials Science and Engineering, The University of Sheffield, Sheffield S1 3JD, U.K.*

Stefano Agrestini − *Diamond Light Source Ltd, Didcot OX11 0DE, U.K.;* ● orcid.org/0000-0002-3625-880X

Veronica Celorrio − *Diamond Light Source Ltd, Didcot OX11 0DE, U.K.;* ● orcid.org/0000-0002-2818-3844

Gabriel E. Pérez − *ISIS Neutron and Muon Source, Rutherford Appleton Laboratory, Didcot OX11 0QX, U.K.;* ● orcid.org/0000-0003-3150-8467

Samuel G. Booth − *The Faraday Institution, Didcot OX11 0RA, U.K.; Department of Materials Science and Engineering, The University of Sheffield, Sheffield S1 3JD, U.K.*

Jordi Cabana − *Department of Chemistry, University of Illinois at Chicago, Chicago, Illinois 60607, United States;* ● orcid.org/0000-0002-2353-5986

Serena A. Cussen − *The Faraday Institution, Didcot OX11 0RA, U.K.; School of Chemistry, University College Dublin, Dublin 4, Ireland;* ● orcid.org/0000-0002-9303-4220

Complete contact information is available at:
https://pubs.acs.org/10.1021/acsenergylett.4c02031

Notes

The authors declare no competing financial interest.

■ REFERENCES

(1) Dose, W. M.; Li, W.; Temprano, I.; O'Keefe, C. A.; Mehdi, B. L.; De Volder, M. F. L.; Grey, C. P. Onset Potential for Electrolyte Oxidation and Ni-Rich Cathode Degradation in Lithium-Ion Batteries. *ACS Energy Lett.* **2022**, 7 (10), 3524−3530.

(2) Zhang, H.; Liu, H.; Piper, L. F. J.; Whittingham, M. S.; Zhou, G. Oxygen Loss in Layered Oxide Cathodes for Li-Ion Batteries: Mechanisms, Effects, and Mitigation. *Chem. Rev.* **2022**, 122 (6), 5641−5681.

(3) Zhang, S. S. Problems and Their Origins of Ni-Rich Layered Oxide Cathode Materials. *Energy Storage Mater.* **2020**, 24, 247−254.

(4) Zhang, M.; Kitchaev, D. A.; Lebens-Higgins, Z.; Vinckeviciute, J.; Zuba, M.; Reeves, P. J.; Grey, C. P.; Whittingham, M. S.; Piper, L. F. J.; Van der Ven, A.; Meng, Y. S. Pushing the Limit of 3d Transition Metal-Based Layered Oxides That Use Both Cation and Anion Redox for Energy Storage. *Nat. Rev. Mater.* **2022**, 7 (7), 522−540.

(5) Gent, W. E.; Abate, I. I.; Yang, W.; Nazar, L. F.; Chueh, W. C. Design Rules for High-Valent Redox in Intercalation Electrodes. *Joule* **2020**, 4 (7), 1369−1397.

(6) Menon, A. S.; Ogley, M. J. W.; Genreith-Schriever, A. R.; Grey, C. P.; Piper, L. F. J. Oxygen Redox in Alkali-Ion Battery Cathodes. *Annu. Rev. Mater. Res.* **2024**, 54, 9.1−9.23.

(7) Genreith-Schriever, A. R.; Banerjee, H.; Menon, A. S.; Bassey, E. N.; Piper, L. F. J.; Grey, C. P.; Morris, A. J. Oxygen Hole Formation Controls Stability in LiNiO2 Cathodes. *Joule* **2023**, 7 (7), 1623−1640.

(8) Bisogni, V.; Catalano, S.; Green, R. J.; Gibert, M.; Scherwitzl, R.; Huang, Y.; Strocov, V. N.; Zubko, P.; Balandeh, S.; Triscone, J. M.; Sawatzky, G.; Schmitt, T. Ground-State Oxygen Holes and the Metal-Insulator Transition in the Negative Charge-Transfer Rare-Earth Nickelates. *Nat. Commun.* **2016**, 7, 1−8.

(9) van Elp, J.; Searle, B. G.; Sawatzky, G. A.; Sacchi, M. Ligand Hole Induced Symmetry Mixing of D8 States in LixNi1-xO, as Observed in Ni 2p x-Ray Absorption Spectroscopy. *Solid State Commun.* **1991**, 80 (1), 67−71.

(10) van Veenendaal, M. A.; Sawatzky, G. A. Doping Dependence of Ni 2 p X-Ray-Absorption Spectra of M x Ni 1 − x O (M = Li, Na). *Phys. Rev. B* **1994**, 50 (16), 11326.

(11) Van Elp, J.; Eskes, H.; Kuiper, P.; Sawatzky, G. A. Electronic Structure of Li-Doped NiO. *Phys. Rev. B* **1992**, 45 (4), 1612−1622.

(12) Huang, H.; Chang, Y. C.; Huang, Y. C.; Li, L.; Komarek, A. C.; Tjeng, L. H.; Orikasa, Y.; Pao, C. W.; Chan, T. S.; Chen, J. M.; Haw, S. C.; Zhou, J.; Wang, Y.; Lin, H. J.; Chen, C. Te; Dong, C. L.; Kuo, C. Y.; Wang, J. Q.; Hu, Z.; Zhang, L. Unusual Double Ligand Holes as Catalytic Active Sites in LiNiO2. *Nat. Commun.* **2023**, 14 (1), 2112.

(13) Ogley, M. J. W.; Menon, A. S.; Pandey, G.; Fajardo, G. J. P.; Johnston, B. J.; McClelland, I.; Majherova, V.; Huband, S.; Tripathy, D.; Temprano, I.; Agrestini, S.; Celorrio, V.; Pérez, G. E.; Booth, S. G.; Grey, C. P.; Cussen, S. A.; Piper, L. F. J. Metal−Ligand Redox in Layered Oxide Cathodes for Li-Ion Batteries. *ChemRXiv* **2024**, DOI: 10.26434/chemrxiv-2024-w906n.

(14) Menon, A. S.; Johnston, B. J.; Booth, S. G.; Zhang, L.; Kress, K.; Murdock, B.; Paez, G.; Anthonisamy, N. N.; Ruiz, N. T.; Agrestini, S.; Zhou, K.; Thakur, P. K.; Lee, T. L.; Nedoma, A. J.; Cussen, S. A.; Piper, L. F. J. Oxygen-Redox Activity in Non-Li-Excess W-Doped LiNiO 2 Cathode. *PRX Energy* **2023**, 2, 013005.

(15) Li, N.; Sallis, S.; Papp, J. K.; Wei, J.; McCloskey, B. D.; Yang, W.; Tong, W. Unraveling the Cationic and Anionic Redox Reactions in a Conventional Layered Oxide Cathode. *ACS Energy Lett.* **2019**, 4 (12), 2836−2842.

(16) Li, W.; Asl, H. Y.; Xie, Q.; Manthiram, A. Collapse of LiNi1- YCoxMnyO2 Lattice at Deep Charge Irrespective of Nickel Content in Lithium-Ion Batteries. *J. Am. Chem. Soc.* **2019**, 141 (13), 5097−5101.

(17) Kondrakov, A. O.; Geßwein, H.; Galdina, K.; De Biasi, L.; Meded, V.; Filatova, E. O.; Schumacher, G.; Wenzel, W.; Hartmann, P.; Brezesinski, T.; Janek, J. Charge-Transfer-Induced Lattice Collapse in Ni-Rich NCM Cathode Materials during Delithiation. *J. Phys. Chem. C* **2017**, 121, 2438124388.

(18) Mikheenkova, A.; Mukherjee, S.; Hirsbrunner, M.; Törnblom, P.; Tai, C. W.; Segre, C. U.; Ding, Y.; Zhang, W.; Asmara, T. C.; Wei, Y.; Schmitt, T.; Rensmo, H.; Duda, L.; Hahlin, M. The Role of

Oxygen in Automotive Grade Lithium-Ion Battery Cathodes: An Atomistic Survey of Ageing. *J. Mater. Chem. A Mater.* **2024**, *12* (4), 2465−2478.

(19) Juelsholt, M.; Chen, J.; Pérez-Osorio, M. A.; Rees, G. J.; De Sousa Coutinho, S.; Maynard-Casely, H. E.; Liu, J.; Everett, M.; Agrestini, S.; Garcia-Fernandez, M.; Zhou, K. J.; House, R. A.; Bruce, P. G. Does Trapped O2 Form in the Bulk of LiNiO2 during Charging? *Energy Environ. Sci.* **2024**, *17*, 2530−2540.

(20) Hennies, F.; Pietzsch, A.; Berglund, M.; Föhlisch, A.; Schmitt, T.; Strocov, V.; Karlsson, H. O.; Andersson, J.; Rubensson, J. E. Resonant Inelastic Scattering Spectra of Free Molecules with Vibrational Resolution. *Phys. Rev. Lett.* **2010**, *104* (19), 1−4.

(21) House, R. A.; Rees, G. J.; Pérez-Osorio, M. A.; Marie, J. J.; Boivin, E.; Robertson, A. W.; Nag, A.; Garcia-Fernandez, M.; Zhou, K. J.; Bruce, P. G. First-Cycle Voltage Hysteresis in Li-Rich 3d Cathodes Associated with Molecular O2 Trapped in the Bulk. *Nat. Energy* **2020**, *5* (10), 777−785.

(22) Wang, L.; Maxisch, T.; Ceder, G. A First-Principles Approach to Studying the Thermal Stability of Oxide Cathode Materials. *Chem. Mater.* **2007**, *19* (3), 543−552.

(23) Cen, J.; Zhu, B.; Scanlon, D. O. Exploring Battery Cathode Materials in the Li-Ni-O Phase Diagrams Using Structure Prediction. *J. Phys. Energy* **2023**, *5*, 035005.

(24) Van der Ven, A.; Ceder, G. Electrochemical Properties of Spinel LixCoO2: A First-Principles Investigation. *Phys. Rev. B Condens Matter Mater. Phys.* **1999**, *59* (2), 742−749.

(25) Arai, H.; Okada, S.; Sakurai, Y.; Yamaki, J. I. Thermal Behavior of Li1-YNiO2 and the Decomposition Mechanism. *Solid State Ion* **1998**, *109* (3−4), 295−302.

(26) Guilmard, M.; Croguennec, L.; Delmas, C. Thermal Stability of Lithium Nickel Oxide Derivatives. Part 1. Li x Ni 0.70 Co 0.15 Al 0.15 O 2 and Li x Ni 0.90 Mn 0.10 O 2 (x = 0.50 and 0.30). *Chem. Mater.* **2004**, *35* (4), 4476−4483.

(27) Wang, C.; Han, L.; Zhang, R.; Cheng, H.; Mu, L.; Kisslinger, K.; Zou, P.; Ren, Y.; Cao, P.; Lin, F.; Xin, H. L. Resolving Atomic-Scale Phase Transformation and Oxygen Loss Mechanism in Ultrahigh-Nickel Layered Cathodes for Cobalt-Free Lithium-Ion Batteries. *Matter* **2021**, *4* (6), 2013−2026.

(28) Bak, S. M.; Nam, K. W.; Chang, W.; Yu, X.; Hu, E.; Hwang, S.; Stach, E. A.; Kim, K. B.; Chung, K. Y.; Yang, X. Q. Correlating Structural Changes and Gas Evolution during the Thermal Decomposition of Charged LixNi0.8Co0.15Al 0.05O2 Cathode Materials. *Chem. Mater.* **2013**, *25* (3), 337−351.

(29) de Biasi, L.; Schiele, A.; Roca-Ayats, M.; Garcia, G.; Brezesinski, T.; Hartmann, P.; Janek, J. Phase Transformation Behavior and Stability of LiNiO2 Cathode Material for Li-Ion Batteries Obtained from In Situ Gas Analysis and Operando X-Ray Diffraction. *ChemSusChem* **2019**, *12* (10), 2240−2250.

(30) Dahn, J. R.; Fuller, E. W.; Obrovac, M.; von Sacken, U. Thermal Stability of LixCoO2, LixNiO2 and λ-MnO2 and Consequences for the Safety of Li-Ion Cells. *Solid State Ion* **1994**, *69* (3−4), 265−270.

(31) Morales, J.; Pérez-Vicente, C.; Tirado, J. L. Thermal Behaviour of Chemically Deintercalated Li1−1Ni1+xO2. *J. Therm. Anal.* **1992**, *38* (3), 295−301.

(32) Arai, H.; Tsuda, M.; Saito, K.; Hayashi, M.; Takei, K.; Sakurai, Y. Structural and Thermal Characteristics of Nickel Dioxide Derived from LiNiO2. *J. Solid State Chem.* **2002**, *163* (1), 340−349.

(33) Squires, A. G.; Ganeshkumar, L.; Savory, C. N.; Kavanagh, S. R.; Scanlon, D. O. Oxygen Dimerization as a Defect-Driven Process in Bulk LiNiO2. *ACS Energy Lett.***2024**, *9*−4180−4187. DOI: .

(34) Bianchini, M.; Schiele, A.; Schweidler, S.; Sicolo, S.; Fauth, F.; Suard, E.; Indris, S.; Mazilkin, A.; Nagel, P.; Schuppler, S.; Merz, M.; Hartmann, P.; Brezesinski, T.; Janek, J. From LiNiO2to Li2NiO3: Synthesis, Structures and Electrochemical Mechanisms in Li-Rich Nickel Oxides. *Chem. Mater.* **2020**, *32* (21), 9211−9227.

(35) Tabuchi, M.; Kuriyama, N.; Takamori, K.; Imanari, Y.; Nakane, K. Appearance of Lithium-Excess LiNiO 2 with High Cyclability Synthesized by Thermal Decomposition Route from LiNiO2

(36) Gottschall, R.; Schöllhorn, R.; Muhler, M.; Jansen, N.; Walcher, D.; Gütlich, P. Electronic State of Nickel in Barium Nickel Oxide, BaNiO3. *Inorg. Chem.* **1998**, *37* (7), 1513−1518.

(37) Rana, J.; Papp, J. K.; Lebens-Higgins, Z.; Zuba, M.; Kaufman, L. A.; Goel, A.; Schmuch, R.; Winter, M.; Whittingham, M. S.; Yang, W.; McCloskey, B. D.; Piper, L. F. J. Quantifying the Capacity Contributions during Activation of Li2MnO3. *ACS Energy Lett.* **2020**, *5* (2), 634−641.

(38) Zuba, M. J.; Grenier, A.; Lebens-Higgins, Z.; Fajardo, G. J. P.; Li, Y.; Ha, Y.; Zhou, H.; Whittingham, M. S.; Yang, W.; Meng, Y. S.; Chapman, K. W.; Piper, L. F. J. Whither Mn Oxidation in Mn-Rich Alkali-Excess Cathodes? *ACS Energy Lett.* **2021**, *6* (3), 1055−1064.

(39) Seo, D. H.; Lee, J.; Urban, A.; Malik, R.; Kang, S.; Ceder, G. The Structural and Chemical Origin of the Oxygen Redox Activity in Layered and Cation-Disordered Li-Excess Cathode Materials. *Nat. Chem.* **2016**, *8* (7), 692−697.

(40) Gent, W. E.; Lim, K.; Liang, Y.; Li, Q.; Barnes, T.; Ahn, S. J.; Stone, K. H.; McIntire, M.; Hong, J.; Song, J. H.; Li, Y.; Mehta, A.; Ermon, S.; Tyliszczak, T.; Kilcoyne, D.; Vine, D.; Park, J. H.; Doo, S. K.; Toney, M. F.; Yang, W.; Prendergast, D.; Chueh, W. C. Coupling between Oxygen Redox and Cation Migration Explains Unusual Electrochemistry in Lithium-Rich Layered Oxides. *Nat. Commun.* **2017**, *8*, 2091 DOI: 10.1038/s41467-017-02041-x.

(41) House, R. A.; Marie, J. J.; Pérez-Osorio, M. A.; Rees, G. J.; Boivin, E.; Bruce, P. G. The Role of O2 in O-Redox Cathodes for Li-Ion Batteries. *Nat. Energy* **2021**, *6* (8), 781−789.

(42) Fukazawa, Y. In Situ X - Ray Absorption Spectroscopy Study of Li(1-z)Ni(1-z)O2 (*z* < 0.02) Cathode Material. *J. Electrochem. Soc.* **2000**, *147*, 2104−2109.

(43) Qiao, R.; Chuang, Y. De.; Yan, S.; Yang, W. Soft X-Ray Irradiation Effects of Li2O2, Li2CO3 and Li2O Revealed by Absorption Spectroscopy. *PLoS One* **2012**, *7*, e49182.

(44) Peng, H. Y.; Li, Y. F.; Lin, W. N.; Wang, Y. Z.; Gao, X. Y.; Wu, T. Deterministic Conversion between Memory and Threshold Resistive Switching via Tuning the Strong Electron Correlation. *Sci. Rep* **2012**, *2*. DOI: DOI: 10.1038/srep00442.

(45) Pan, G.; He, G.; Zhang, M.; Zhou, Q.; Tyliszczak, T.; Tai, R.; Guo, J.; Bi, L.; Wang, L.; Zhang, H. Nanobubbles at Hydrophilic Particle-Water Interfaces. *Langmuir* **2016**, *32* (43), 11133−11137.

(46) House, R. A.; Maitra, U.; Pérez-Osorio, M. A.; Lozano, J. G.; Jin, L.; Somerville, J. W.; Duda, L. C.; Nag, A.; Walters, A.; Zhou, K. J.; Roberts, M. R.; Bruce, P. G. Superstructure Control of First-Cycle Voltage Hysteresis in Oxygen-Redox Cathodes. *Nature* **2020**, *577* (7791), 502−508.

(47) Qiao, R.; Wray, L. A.; Kim, J. H.; Pieczonka, N. P. W.; Harris, S. J.; Yang, W. Direct Experimental Probe of the Ni(II)/Ni(III)/Ni(IV) Redox Evolution in LiNi0.5Mn1.5O4 Electrodes. *J. Phys. Chem. C* **2015**, *119* (49), 27228−27233.

(48) Fehse, M.; Etxebarria, N.; Otaegui, L.; Cabello, M.; Martín-Fuentes, S.; Cabañero, M. A.; Monterrubio, I.; Elkjær, C. F.; Fabelo, O.; Enkubari, N. A.; López Del Amo, J. M.; Casas-Cabanas, M.; Reynaud, M. Influence of Transition-Metal Order on the Reaction Mechanism of LNMO Cathode Spinel: An Operando X-Ray Absorption Spectroscopy Study. *Chem. Mater.* **2022**, *34* (14), 6529−6540.

(49) Kim, J.-H.; Myung, S.-T.; Yoon, C. S.; Kang, S. G.; Sun, Y.-K. Comparative Study of LiNi 0.5 Mn 1.5 O 4-δ and LiNi 0.5 Mn 1.5 O 4 Cathodes Having Two Crystallographic Structures: Fd3m and P4 332. *Chem. Mater* **2004**, *35* (21), 906−914.

(50) Jung, R.; Metzger, M.; Maglia, F.; Stinner, C.; Gasteiger, H. A. Oxygen Release and Its Effect on the Cycling Stability of LiNixMnyCozO2 (NMC) Cathode Materials for Li-Ion Batteries. *J. Electrochem. Soc.* **2017**, *164* (7), A1361−A1377.

(51) Massel, F.; Aktekin, B.; Liu, Y. S.; Guo, J.; Sørby, M. H.; Brandell, D.; Younesi, R.; Hahlin, M.; Duda, L. C. The Role of Anionic Processes in Li1−xNi0.44Mn1.56O4 Studied by Resonant Inelastic X-Ray Scattering. *Energy Advances* **2023**, *2* (3), 375−384.